A Kinetic Modeling of the Liquid-Phase Oxidation of Lactose Over Pt- and Au-Supported Catalysts

C. I. Meyer, S. A. Regenhardt, J. Zelin, V. Sebastian, A. J. Marchi & T. F. Garetto

Topics in Catalysis

ISSN 1022-5528
Volume 59
Combined 2-4

Top Catal (2016) 59:168-177
DOI 10.1007/s11244-015-0427-4

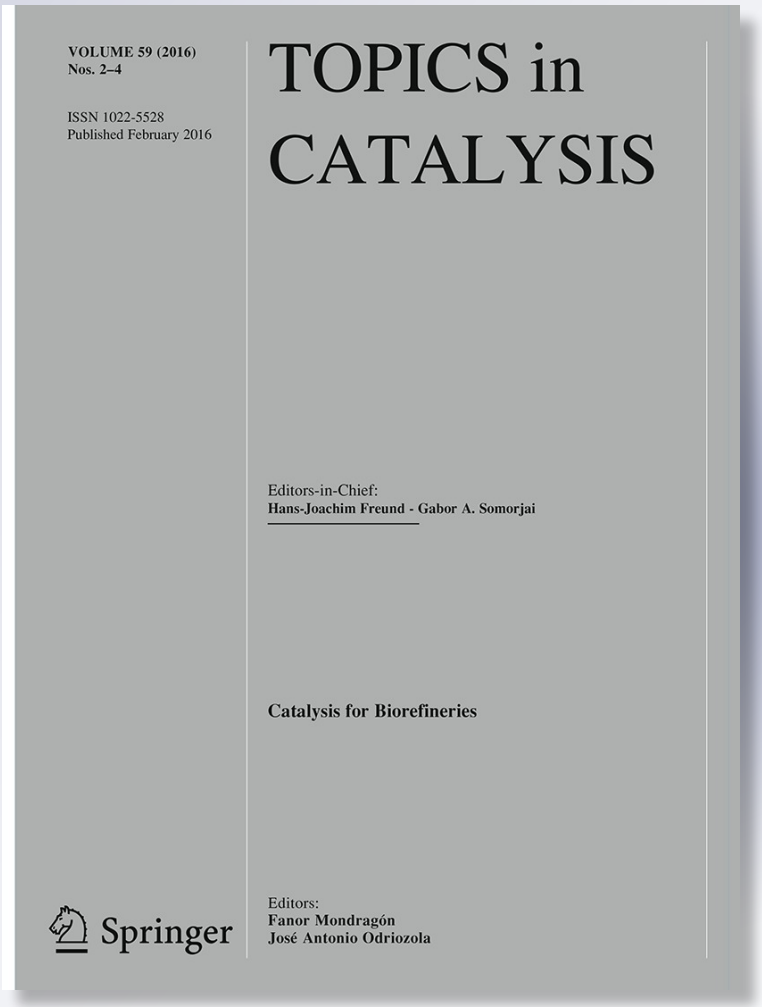

Springer

Top Catal (2016) 59:168–177
DOI 10.1007/s11244-015-0427-4

ORIGINAL PAPER

A Kinetic Modeling of the Liquid-Phase Oxidation of Lactose Over Pt- and Au-Supported Catalysts

C. I. Meyer[1] · S. A. Regenhardt[1] · J. Zelin[1] · V. Sebastian[2,3] · A. J. Marchi[1] · T. F. Garetto[1]

Published online: 30 July 2015

Abstract Pt and Au catalysts, 2 wt% metal loading, supported on SiO_2 and Al_2O_3 were used to study the effect of metal and support on the liquid-phase oxidation of lactose. Pt-based catalysts were prepared by incipient wetness impregnation while Au-based catalysts were obtained by the precipitation-deposition method. Catalytic tests were carried out in aqueous phase at 65 °C, using O_2 as oxidizing agent and keeping pH constant at 9 by controlled addition of NaOH aqueous solution. In all of the cases, the only product of reaction detected and quantified was lactobionic acid. It was found that Pt supported on Al_2O_3 was more active than Pt supported on SiO_2. This was explained on the basis that metal Pt dispersion on Al_2O_3 was three times higher than on SiO_2. At the same time, Au/Al_2O_3 catalyst was more active than Pt/Al_2O_3 catalysts. The higher activity of Au/Al_2O_3 was attributed to Au nanoparticles interacting with the support, as determined by transmission electron microscopy. It was also verified that Au/Al_2O_3 activity was almost the same after two consecutive runs, indicating a good stability of the Au active phase. Kinetic studies were carried out by varying the initial concentration of lactose in the reaction mixture. A negative order respect to the reactant, determined applying a pseudo-homogeneous model, was estimated, which indicates that lactose molecules are strongly adsorbed on the surface of metal Au nanoparticles. A LHHW model, assuming that oxygen chemisorption was the controlling step, allowed to explain the negative order respect to lactose.

Keywords Lactose · Lactobionic acid · Noble metal catalysts · Kinetic modeling

1 Introduction

Lactose (LA) is a major component of whey, the main by-product in the cheese production of dairy industry. Only a small part of the large volume of whey obtained in the dairy industry is processed to obtain LA. The remaining whey is treated as a waste. Several processes have been developed in order to add value to LA. Some of them are electrochemical or catalytic and other are microbiological processes [1–3]. Cheese whey typically contains about 5 wt% lactose, which can be converted to added value compounds by hydrogenation and oxidation reactions. For example, lactitol can be produced by catalytic hydrogenation of LA. This poliol is used as a sugar substitute in dietetic products [4]. Other possibility is to convert LA to lactobionic acid (LB) by selective catalytic oxidation (Scheme 1). Nowadays, LB can be produced by microbiological oxidation of LA. The main disadvantages of this process are the long times required to achieve high levels of conversion and the formation of hydrogen peroxide as a by-product [5]. This α-hydroxy acid has antioxidant properties and its largest commercial use is as an important constituent of solutions employed to preserve human

✉ T. F. Garetto
tgaretto@fiq.unl.edu.ar

[1] Catalysis Science and Engineering Research Group (GICIC), INCAPE, UNL-CONICET, Colectora Ruta Nac. No 168 km. 0, 3000 Santa Fe, Argentina

[2] Department of Chemical Engineering, Aragon Institute of Nanoscience (INA), University of Zaragoza, Campus Río Ebro-Edificio I+D, C/ Poeta Mariano Esquillor S/N, 50018 Zaragoza, Spain

[3] CIBER de Bioingeniería, Biomateriales y Nanomedicina (CIBER-BBN), C/Monforte de Lemos 3-5, Pabellón 11, 28029 Madrid, Spain

Scheme 1 Oxidation of lactose (LA) to lactobionic acid (LB) and subsequent dehydrogenation-oxidation

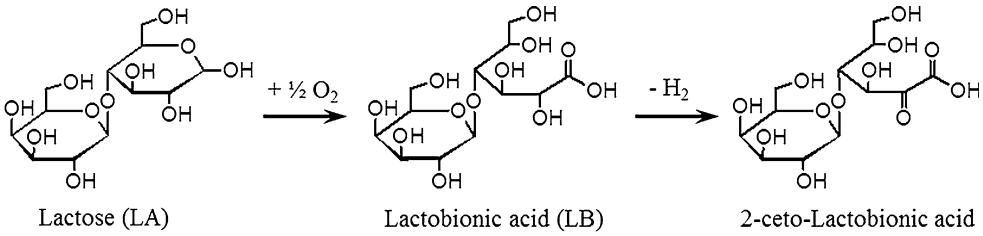

organs during transplantation procedures [6]. LB is also employed as acidulant, complexing agent and antioxidant in food and pharmaceuticals. It is also well known that the LA hydrolysis gives the corresponding monosaccharides: galactose and glucose. Other products of industrial interest can be obtained from these two sugars, e.g., gluconic acid, glucaric and glucuronic acid can be produced by glucose oxidation.

Recently, there has been an increasing interest in the LB production by heterogeneous catalytic oxidation of LA. Some authors have studied the catalytic oxidation of different mono and disaccharides using several metals and supports. Pt and Pd-based catalysts, in some cases promoted with Bi, were used to carry out the oxidation of sugars [7–9]. Some deactivation of these catalysts was observed, which was assigned to overoxidation of the metal surface [5]. LA oxidation has been studied employing Au-based catalysts on inert and reducible supports with different acidic properties [6, 8]. Bulk Au is not a good catalyst, but Au nanoparticles or well dispersed Au are active in catalytic oxidation reactions. For example, the oxidation of CO occurs at low temperature over Au nanoparticles [10–12]. Gold nanoparticles can be formed when the deposition–precipitation method is used to prepare supported Au catalysts. Centeno et al. [13, 14] have studied the CO oxidation employing Au-based catalysts, which were prepared using different supports. By FTIR studies, they observed that when gold is deposited on Al_2O_3 and then reoxidize, a couple Au^+/Au^0 operates in the CO oxidation over Au/Al_2O_3 catalysts. Murzina et al. [6] found that type of metal, pH of reaction medium, temperature and O_2 concentration have an important influence on the LA oxidation in liquid-phase. From the analysis of concentration–time curves, using Au on different supports, such as, SiO_2, Al_2O_3, ZrO_2, they claimed that the order respect to lactose was zero, but they did not mentioned the effect of the initial LA concentration on the reaction rate. To our knowledge, there are not works in which a detailed kinetic modeling is discussed.

In this work, we analyse the effect of support, metal and initial reactant concentration in the liquid-phase on the LA oxidation at low temperature (65 °C) and pH 9 in order to determine the conditions that allow to obtain high yield and selectivity to LB. In addition, we performed a kinetic modeling of the experimental data obtained with Au (2 wt%)/Al_2O_3 with the aim of getting an insight into the LA oxidation mechanism over a well-dispersed metal Au phase.

2 Experimental

2.1 Catalyst Preparation

Both Pt and Au samples were prepared by different methods in order to obtain approximately 2 wt% of metal loading in the final catalysts.

Pt/SiO_2 and Pt/Al_2O_3 precursors were prepared by the incipient wetness impregnation method. Pt was deposited on commercial silica (Sigma-Aldrich grade 62, Sg = 270 $m^2\ g^{-1}$, Vp = 0.88 $cm^3\ g^{-1}$, dp = 13.9 nm) or commercial γ-Al_2O_3 (Cyanamid Ketjen CK 300, Sg = 190 $m^2\ g^{-1}$, Vp = 0.49 $cm^3\ g^{-1}$, dp = 9.96 nm), previously calcined at 600 °C, by adding dropwise a 0.02 mol L^{-1} aqueous solution of H_2PtCl_6 (Sigma-Aldrich 99.99 %). The catalytic precursor was dried at 100 °C for 12 h and then calcined in air flow at 500 °C during 4 h. Finally, the samples were reduced in H_2 flow at 300 °C for 4 h.

Au/Al_2O_3 precursor was prepared by the precipitation-deposition method [13]. $HAuCl_4{\cdot}3H_2O$ (Sigma-Aldrich, 99.99 %) was added to a fixed volume of deionized water in order to obtain a catalytic precursor with 2 wt% metal loading. The initial pH of the solution was 1.5 and it was then adjusted to 7.0 by adding dropwise 0.1 mol L^{-1} NaOH aqueous solution. The yellowish solution was heated at 70 °C and then Al_2O_3 was added under continuous stirring. The slurry was stirred for 1 h more at 70 °C. Afterwards, the suspension was filtered and the solid sample was separated from a colourless solution. The hydrated precursor was washed with deionized water several times until Na^+ and Cl^- ions were not detected in the washing water. Then, the sample was dried at 50 °C during 12 h and finally calcined in air at 500 °C during 2 h.

2.2 Sample Characterization

Metal loading of samples was determined by inductively coupled plasma (ICP) using a Perkin Elmer OPTIMA 2100

equipment. Specific surface area (Sg), pore volume (Vp) and mean pore diameter (d_P) were measured by N_2 physisorption at −196 °C in a Quantachrome Autosorb I sorptometer. The BET equation was applied to estimate specific surface area and the BJH method for pore distribution calculations. The identification of polycrystalline species was carried out by X-ray diffraction (XRD) using a Shimadzu XD-1 diffractometer and Ni-filtered Cu-Kα radiation with a scan speed of 2° min^{-1}. The average crystallite sizes on Pt-supported samples were calculated by applying the Scherrer equation and considering the Pt(111) diffraction lines.

The platinum dispersion (D_{Pt}) on Pt/SiO_2 and Pt/Al_2O_3 was determined by H_2 chemisorption at room temperature using a conventional vacuum unit. Samples were reduced in H_2 at 300 °C for 2 h and then outgassed for 2 h at the same temperature prior to performing gas chemisorption experiments. Hydrogen uptake was determined using the double isotherm method as detailed in a previous work [15].

Electron microscopy observations were carried out at the LMA-INA-UNIZAR facilities using a 200 kV G2 20 S-Twin Tecnai microscope equipped with a LaB6 electron source with a "SuperTwin®" objective lens allowing resolution of 0.24 nm. High angle annular dark field scanning transmission electron microscopy (HAADF-STEM) were performed on a Tecnai G2-F30 Field Emission Gun microscope with a super-twin lens and 0.2 nm point-to-point resolution and 0.1 line resolution operated at 300 kV. HAADF detector enables to acquire HAADF-STEM images with atomic number contrast for high scattering angles of the electrons (Z-contrast). To prepare the samples for electron microscopy observation, sample powder was dispersed in milli-Q water. After 30 s in an ultrasonic bath, a drop of this suspension was applied to a copper grid (200 mesh) coated with carbon film, and allowed to dry in air.

2.3 Catalytic Tests

The liquid-phase oxidation of LA (Aldrich, 99 %) was carried out in a thermostated and stirred (1000 rpm max.) glass reactor at atmospheric pressure. The reactor was loaded with 300 mL of water and 1 g of catalyst. The temperature was adjusted at 65 °C while N_2 was bubbled in order to remove the dissolved oxygen. Once the system reached the reaction temperature, a LA solution was added and O_2 was fed by air bubbling with a flow rate of 230 cm^3 min^{-1} and the O_2 concentration in the solution was 3.1 mg L^{-1}. Initial LA concentration, $[LA]^0$, was varied between 0.03 and 0.17 mol L^{-1} and the mass of catalyst was the adequate to get a relation $w_{cat}/n_A^0 = 30$ g mol^{-1}. The pH was kept constant at 9 through reaction time by controlled addition of a 1 mol L^{-1} NaOH aqueous solution. Liquid samples were collected from the reactor every 15–30 min by using a micro-syringe so that, less than a 3 % of the total liquid volume was extracted during the run. Samples at different reaction times were taken and analyzed by HPLC using a Phenomenex™ column (Phenosphere 5 micras, NH_2, 80 Å, 250 mm × 4.60 mm) and a Acetonitrile-sodium phosphate buffer (50 mmol L^{-1}, pH 5.0) (60:40) as a mobile phase. The chromatograph was a Shimadzu modular system equipped with dual-pump, fixed-loop (20 µL) injector, a controlled oven and a differential refraction index detector. All solvents were HPLC grade, the water was ultrapurified by an OSMOION equipment and the mobile phases were previously filtrated through a 0.22 µm nylon filter. In all cases, the only compounds detected, analysed and quantified were LA y LB.

3 Results and Discussion

3.1 Sample Characterization

Textural properties of the prepared samples are shown in Table 1. The values obtained for Sg, Vp y dp of metal-supported samples are similar to those of the supports alone. This is indicative that the preparation method has no important influence on the textural properties of the oxides used as supports. Elemental analysis of Pt and Au, carried out by ICP, indicated that experimental metal loading were similar to the theoretical ones. The metal dispersion, determined by hydrogen chemisorption, of Pt/Al_2O_3 was almost twice that of Pt/SiO_2 (Table 1). From these values of dispersion, the mean particle size was calculated assuming cubic shape for metal particles.

The X-ray diffractograms of Pt and Au supported samples are presented in Fig. 1. The peaks corresponding to (111) and (200) planes of metallic platinum with a face-centered cubic crystalline structure [16] were identified in the case of Pt/SiO_2 sample (Fig. 1, curve a). In addition, the amorphous halo attributed to the SiO_2 support was observed in the 2θ range of 15°–30°. An average crystallite size of 6.5 nm was calculated from the full width at half maximum intensity of the Pt(111) peak. The average crystallite size estimated with Scherrer equation was rather similar to the value obtained for the mean particle size by H_2 chemisorption (Table 1), which is indicating that the metal Pt particles are mainly formed by single nanocrystallites, i.e., no crystallite agglomeration occurred during sample preparation.

In the case of Pt/Al_2O_3, the intensity of the peak assigned to Pt (111) planes is much lower than the one observed for Pt/SiO_2 (Fig. 1, curves a, b), which indicates that the crystalline degree of metal Pt phase on Al_2O_3 is lower than on SiO_2. Besides, the average crystallite size

Table 1 Physicochemical characterization of the samples prepared in this work

Sample	Sg (m^2 $g^{-1)}$	Vp (cm^3 g^{-1})	dp (nm)	% Metal	D_{Pt} (%)	Mean particle size (nm)
Pt/SiO_2	261	0.87	13.8	2.3	13	7.5[a]
Pt/Al_2O_3	185	0.47	9.88	2.0	23	4.3[a]
Au/Al_2O_3	180	0.47	9.92	2.1	–	3.7[b]

[a] Calculated from dispersion values, D_{Pt}, determined by H_2 chemisorption

[b] Determined by statistical counting of approximately 300 particles from TEM micrographies

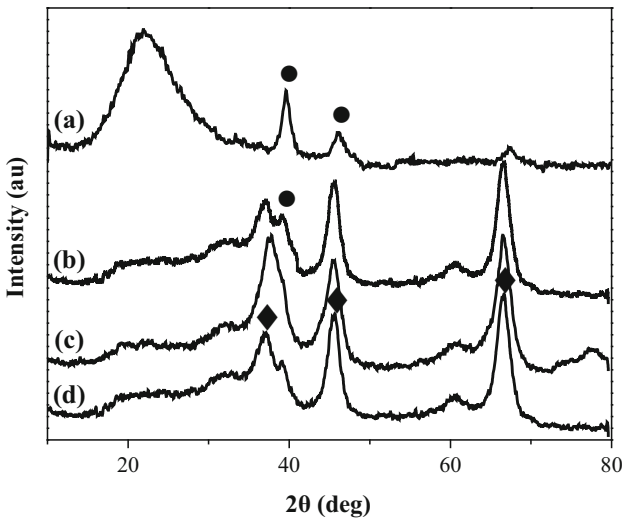

Fig. 1 XRD diffractograms of reduced samples and Al_2O_3 support. *a* Pt/SiO_2; *b* Pt/Al_2O_3; *c* Au/Al_2O_3; *d* Al_2O_3. *Black circle* diffraction lines from metallic Pt (111) and (200) family planes; *black diamond suit* diffraction lines from γ-Al_2O_3 crystalline structure

could not be determined by applying Scherrer equation since this small diffraction peak was overlapping the diffraction peak centered at $2\theta = 38°$ arising from the crystalline structure of the support (Fig. 1, curve d). The mean particle size determined from H_2 chemisorption was around 4.3 nm (Table 1), which is precisely the limit for detection of crystalline domains by XRD [16]. This is in agreement with the broad peak of low intensity observed for the metal Pt phase formed on Al_2O_3 (Fig. 1, curve b).

The X-ray diffractogram obtained for Au/Al_2O_3 was similar to that observed with Al_2O_3, the diffraction lines corresponding to the crystalline structure of the support and a very broad peak of very low intensity between $2\theta = 72°$ and 80°, which can be attributed to very small crystallites of metalic Au, were detected (Fig. 1, curves c, d). It is likely that crystalline domains of Au species are just at the limit size to be detected by XRD and even an amorphous Au phase was formed.

TEM and HAADF-STEM images showed that Au/Al_2O_3 samples are composed of metal Au nanoparticles highly dispersed on the support surface (Fig. 2). The particle size distribution and the mean particle size were determined by counting approximately 300 particles (Fig. 3; Table 1). The histogram showed that more than 80 % of the Au nanoparticles are smaller than 4.5 nm and less than 10 % of the nanoparticles are between 5 and 7 nm. The medium size of metal Au particles was 3.7 nm, which is in agreement with the X-ray diffractogram obtained for Au/Al_2O_3 sample.

3.2 Catalytic Tests

The reactant concentration as a function of time during the liquid-phase LA oxidation is shown in Fig. 4a. It can be observed that the three catalysts are active for LA oxidation and the activity pattern is the following: $Au/Al_2O_3 > Pt/Al_2O_3 > Pt/SiO_2$. LA conversions attained at 180 min for Pt/SiO_2 and Pt/Al_2O_3 catalysts were 9 and 23 %, respectively. These results could be explained considering that the metallic dispersion of Pt/Al_2O_3 catalyst was higher than that of Pt/SiO_2 catalyst (Table 1). The LA conversion on Au/Al_2O_3 catalyst at 150 min was 97 %, i.e., much higher than on Pt/Al_2O_3. Taking into account the characterization results, we concluded that, under the experimental conditions used in this work, metal Au nanoparticles dispersed on Al_2O_3 are more active, for the liquid-phase LA oxidation, than metal Pt particles of similar medium size supported on the same insulating oxide. These results are in agreement with those obtained by Murzina et al. [6]. Furthermore, the ICP analysis of reactant mixture samples, taken at the end of the reaction, showed that there is no metal leaching under the experimental conditions used in this work. For all catalysts the only detected and quantified product was LB, showing that both Pt- and Au-based catalysts are highly selectivity in the liquid-phase LA oxidation to LB.

Some possible side reactions that could happen are the isomerization, hydrolysis and disproportionation of LA. Additional experiments were carried out in order to discard the occurrence of any of these reactions with Au/Al_2O_3 catalyst. N_2 was bubbled in the reaction system during the first hour, and no LA conversion was detected. Then, the bubbling of N_2 was switched to air and the oxidation of LA to LB started immediately, i.e., no induction period was observed. Again, the only reaction product detected during the test was LB. Therefore, this experiment confirms that

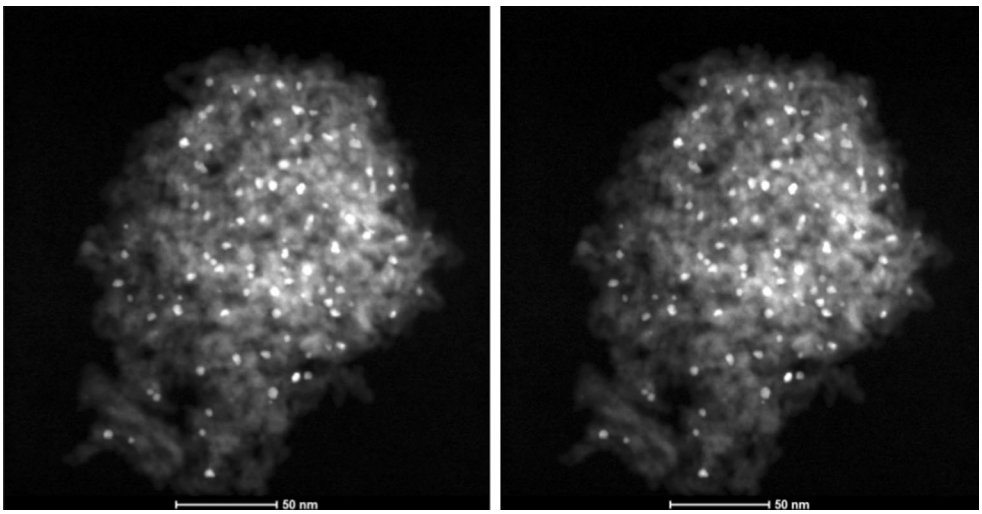

Fig. 2 HAADF-STEM images of Au/Al_2O_3 catalyst

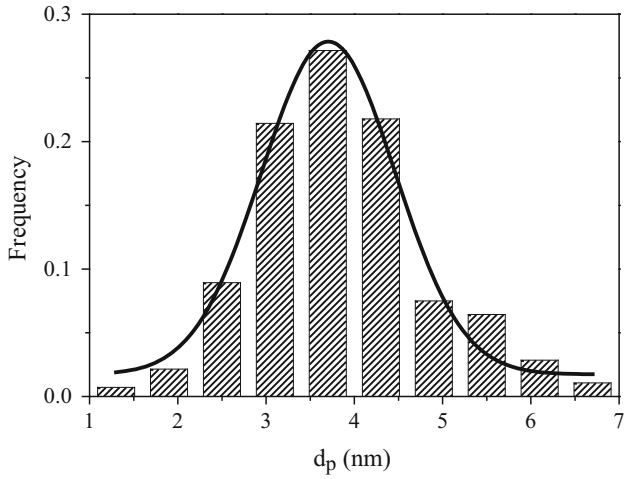

Fig. 3 Histogram of Au particle diameters obtained by counting 300 particles

the Au/Al_2O_3 catalyst is highly selective to LB under the reaction conditions used in this work.

In order to analyze the deactivation of Au/Al_2O_3 catalyst during the liquid-phase oxidation of LA, two consecutive runs under the same conditions were carried out. The evolution of the relative concentration of LA with time is presented in Fig. 4b. In the first run, LA was totally consumed in approximately 2 h. Afterwards, the same amount of the initial LA was added to the reaction system and a similar evolution was observed. This indicates that the deactivation of the Au/Al_2O_3 catalyst during one run was negligible under the reaction conditions used in this work.

The LA conversion over the Au/Al_2O_3 catalyst as a function of the parameter ($w_{cat} \cdot t/n^0_{LA}$) (g min $mmol^{-1}$) is shown in Fig. 5 for different initial concentrations of LA,

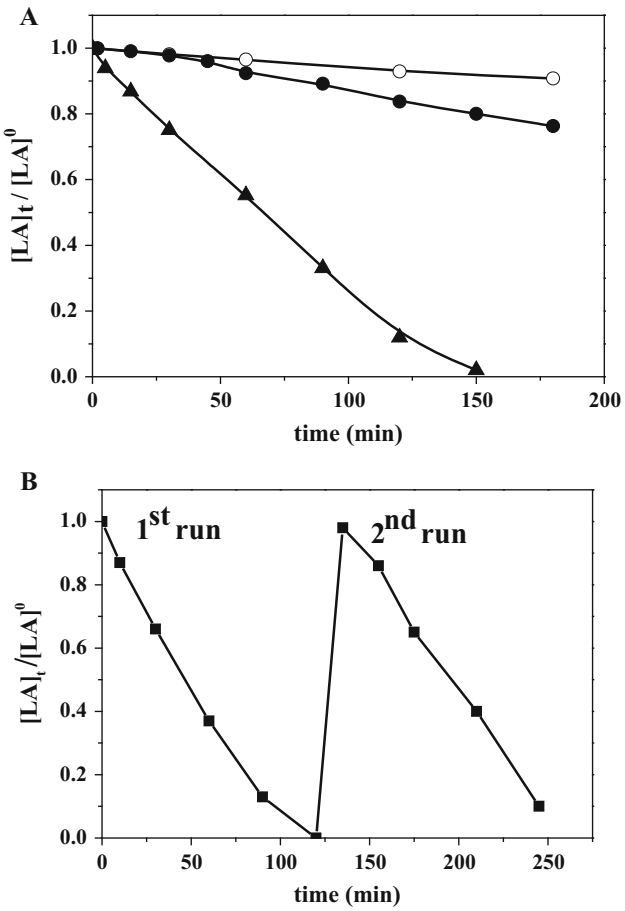

Fig. 4 **a** Relative concentration of lactose ($[LA]/[LA]^0$) as a function of time. T = 65 °C, pH 9, w = 1 g, $[LA]^0 = 0.11$ mol L^{-1}. *White circle* Pt/SiO_2, *black circle* Pt/Al_2O_3, *black up-pointing triangle* Au/Al_2O_3. **b** Conversion of lactose, X_{LA}, as a function of time in two consecutive tests with Au/Al_2O_3 catalyst. T = 65 °C, pH 9, $[LA]^0 = 0.06$ mol L^{-1}

i.e., $[LA]^0$. It can be observed that for a given $[LA]^0$, the reaction rate remains almost constant until LA conversion reached 75–80 %, which is in agreement with an order zero respect to LA [6]. However, as the $[LA]^0$ was increased, the initial oxidation rate and the LA conversion at a given time diminished. These results indicate that the reaction order respect to LA should be negative, which can be explained assuming strong LA adsorption on the surface of the Au nanoparticles [17].

With the aim of getting more evidence about the interaction of LA and LB with the surface of the metal Au nanoparticles, a kinetic modeling was performed. In a first step, the reaction order was estimated by considering a pseudo-homogeneous model. On the basis of the results obtained with this model, a Langmuir–Hinshelwood–Hougen–Watson (LHHW) model was proposed to explain the catalytic behavior observed during liquid-phase LA oxidation on Au/Al_2O_3 catalyst.

3.3 Kinetic Modeling for LA Oxidation on Au(2 %)/Al_2O_3

A semi-batch perfectly mixed reactor was considered for modeling and possible mass transfer limitations were ruled out by selecting an adequate catalyst particle size and stirring speed. Accordingly, a stirring speed of 800 rpm and particle size lower than 75 μm were used to insure that external and intraparticle mass transfer are not controlling the reaction rate. It is important to remark that all experiences for kinetic modeling were performed with a constant O_2 concentration (3.1 mg L^{-1}), a constant ratio w_{cat}/n^0_{LA} (catalyst mass/LA initial moles) and equal to 30 g mol^{-1} and the same fluid dynamics conditions. Under these conditions the mass balance for LA in the reactor can be expressed as presented in Eq. (1) where $(-\hat{r}_{LA})$ is the rate of LA oxidation expressed by catalyst weight unit:

$$(-\hat{r}_{LA}) = -\frac{d[LA]}{[LA]^0 \cdot d\left(\frac{t \cdot w_{cat}}{n^0_{LA}}\right)} \quad (1)$$

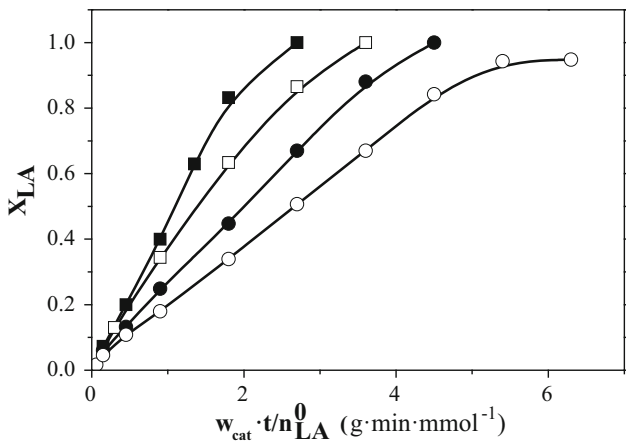

Fig. 5 Lactose conversion, X_{LA}, as a function of parameter $w_{cat} \cdot t/n^0_{LA}$ for different initial lactose concentration, $[LA]^0$, with Au/Al_2O_3 catalyst. T = 65 °C, pH 9, w/n^0_{LA} = 30 g mol^{-1}, *black square* 0.03 mol L^{-1}; *white square* 0.06 mol L^{-1}; *black circle* 0.11 mol L^{-1}; *white circle* 0.17 mol L^{-1}

3.4 Pseudo Homogeneous Potential Model

Firstly, the experimental data were analyzed considering a pseudo-homogeneous model. The pseudo-homogeneous modeling and fitting was performed by linearization of the corresponding power-law expression and calculating the initial reaction rates $(-\hat{r}_{LA})^0$ for every initial LA concentration $[LA]^0$ from experimental data shown in Fig. 5. The linear least square fitting was applied to estimate the parameters of the pseudo-homogeneous model. This approach does not have into account the evolution of the LA concentration or conversion with reaction time.

According to the empirical power-law model, the reaction rate can be expressed as:

$$(-\hat{r}_{LA}) = k \cdot [LA]^n \quad (2)$$

where k is the kinetic constant of reaction and n is the kinetic order with respect to LA. The order n may take virtually all the values: integer, fractional, positive, negative or zero. Elementary reactions have integer orders. However, for the case of non-elementary reactions, the kinetic orders will generally assume fractional values that are only valid within a narrow range of operating conditions where the experiments has been carried out. Equation (2) can be linearized and expressed at initial conditions (t = 0, r^0_{LA} and $[LA]^0$) to obtain Eq. (3). The kinetic parameters, k and n, can be estimated by applying this equation.

$$\ln\left(-\hat{r}^0_{LA}\right) = \ln k + n \cdot \ln\left([LA]^0\right) \quad (3)$$

The values for the initial rate of LA oxidation r^0_{LA} were calculated directly from the slope of the straight lines obtained from X_{LA} versus $w_{cat} \cdot t/n^0_{LA}$ (Fig. 5) for each $[LA]^0$ and considering data at $X_{LA} < 70$ %. The estimate obtained for n by this procedure was -0.43 ± 0.043 with a 95 % confidence. A good fitting between initial rates and initial concentration was found (Fig. 6a). The correlation coefficient, R^2, for the linear regression is 0.9992 and both estimates k and n are significantly different from zero with a 95 % confidence. As can be observed in Fig. 6b, the pseudo-homogeneous potential model fits satisfactorily the experimental data, since a straight line was obtained when the experimental concentrations of LA are represented as a function of the calculated concentrations with the pseudo-homogenous model, until a LA conversion of 70–80 %.

The negative estimate for the reaction order n indicates that LA is strongly adsorbed on the catalytic active sites present on

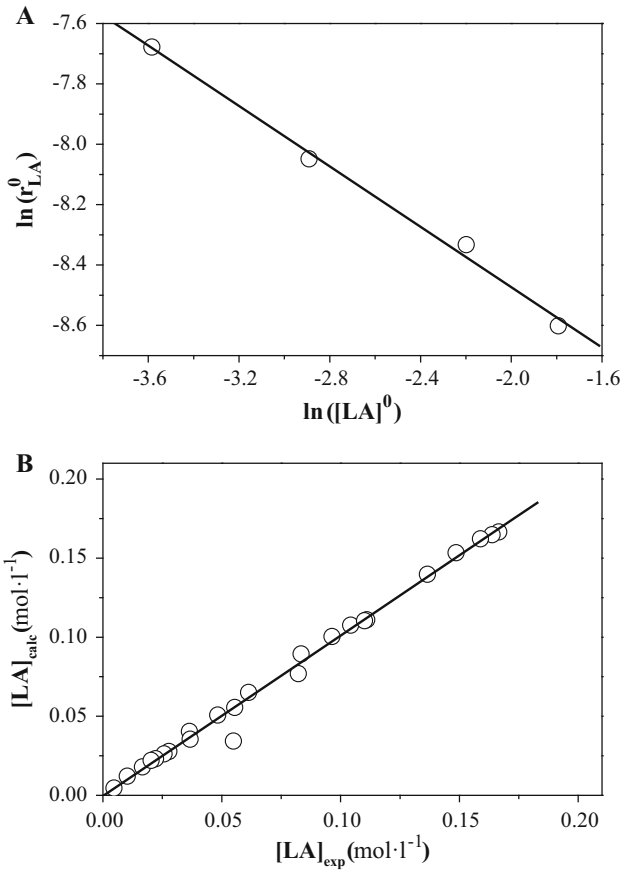

Fig. 6 **a** Double ln-plot and linear fitting of $(-\hat{r}_{LA})^0$ versus $[LA]^0$ for pseudo-homogeneous model with Au/Al_2O_3 catalyst. T = 65 °C, pH 9. **b** Correlation between experimental lactose concentration, $[LA]_{exp}$, and predicted lactose concentration, $[LA]_{calc}$, obtained with pseudo-homogeneous model

the surface of the metal Au nanoparticles. From these results, it was concluded that, for a given initial concentration of LA, the surface sites on metal Au nanoparticles are saturated with LA strongly adsorbed. Then, the LA oxidation occurs as if the reaction order respect to LA is apparently zero. However, as the initial LA concentration was raised, the initial amount of LA strongly adsorbed on the surface of metal Au nanoparticles also increased and so the initial availability of free active sites is lower. In what follows, a heterogeneous modeling will be applied to find more evidence about how the increasing initial concentration of LA produces a decrease in LA oxidation rate.

3.5 Langmuir–Hinselwood–Hougen–Watson (LHHW) Model

Taking into account that the LA oxidation rate for a given $[LA]^0$ was not depending on the LA concentration but it diminished with increasing $[LA]^0$, we decided to propose a LHHW model that explains satisfactorily from both, a physical and statistical point of view, what happened during experiments performed in this work. The hypotheses made for the formulation of the LHHW mechanism used in this work are the following:

- There be only one type of adsorption site (L^*) where LA, LB and O_2 can be adsorbed and react.
- The adsorptions of LA and LB on the catalyst surface are reversible steps in equilibrium.
- The surface reaction between adsorbed LA and O_2 is also in equilibrium.
- According to experimental conditions, the O_2 concentration in liquid phase is constant.
- The O_2 chemisorption on Au nanoparticles is dissociative and it is the controlling step.

This last hypothesis was made on the basis of previous DFT studies in which both, molecular chemisorption, and dissociative chemisorption of O_2 on Au nanoclusters, has been studied [18, 19]. There was found that: (i) Oxygen molecules chemisorb on Au nanoclusters with typical binding energies of 0.5–1.5 eV, (ii) in the lowest energy configuration, the oxygen molecule dissociates into two O atoms. The bonding mechanism involves charge transfer to the oxygen molecule with a concomitant activation of the O–O bond (to a superoxo state), forming a nearly linear O–Au–O bridge. Molecular adsorption occurs with smaller binding energy on cluster with <4 Au atoms, while dissociative adsorption is favored for larger clusters, over 8 Au atoms. These conclusions permit us to propose the O_2 dissociative chemisorption on Au nanoparticles, instead of a non-dissociative one, as the rate controlling step.

Considering the former hypothesis, the main steps for the proposed LHHW reaction mechanism are the following, were the controlling step is the dissociative chemisorption of dissolved O_2 (step iii):

$$\text{(i)}\quad 2LA_{(dis)} + 2L^* \overset{K_{LA}}{\Leftrightarrow} 2LA^* \qquad K_{LA} = \frac{[LA^*]}{[LA_{(dis)}]\cdot[L^*]} \tag{4}$$

$$\text{(ii)}\quad O_{2_{(g)}} \overset{K_H}{\Leftrightarrow} O_{2_{(dis)}} \qquad K_H = \frac{\left[O_{2_{(dis)}}\right]}{\bar{p}_{O_{2_{(g)}}}} \tag{5}$$

$$\text{(iii)}\quad O_{2_{(dis)}} + L^* \overset{(-\hat{r}_{LA})}{\rightarrow} O^* - L - O^* \qquad (-\hat{r}_{LA}) = k^*_{LHHW}\cdot\left[O_{2_{(dis)}}\right]\cdot[L^*] \tag{6}$$

$$\text{(iv)}\quad 2LA^* + O^* - L - O^* \overset{K_S}{\Leftrightarrow} 2LB^* + L^* \qquad K_S = \frac{[LB^*]^2\cdot[L^*]}{[LA^*]^2\cdot[O^* - L - O^*]} \tag{7}$$

$$\text{(v)}\quad 2LB^* \overset{K_{LB}}{\Leftrightarrow} 2L^* + 2LB_{(dis)} \qquad K_{LB} = \frac{[LB^*]}{[LB_{(dis)}]\cdot[L^*]} \tag{8}$$

The balance of the total active sites, C_{TL}, is given by Eq. (9):

$$C_{TL} = [L^*] + [LA^*] + [LB^*] + [O^* - L - O^*] \quad (9)$$

Replacing with Eqs. (4), (5), (7) and (8) in Eq. (9), we obtained Eq. (10):

$$C_{TL} = [L^*]\left\{1 + K_{LA} \cdot \left[LA_{(dis)}\right] + K_{LB} \cdot \left[LB_{(dis)}\right] + \frac{K_{LB}^2}{K_S \cdot K_{LA}^2} \cdot \left[\frac{LB_{(dis)}}{LA_{(dis)}}\right]^2\right\} \quad (10)$$

Substituting with Eq. (10) and Henry law, Eqs. (5), in (6), the reaction rate can be expressed as follows:

$$(-\hat{r}_{LA}) = \frac{k^*_{LHHW} \cdot K_H \cdot \bar{p}_{O_{2(g)}} \cdot C_{TL}}{\left\{1 + K_{LA} \cdot \left[LA_{(dis)}\right] + K_{LB} \cdot \left[LB_{(dis)}\right] + \frac{K_{LB}^2}{K_S \cdot K_{LA}^2} \cdot \left[\frac{LB_{(dis)}}{LA_{(dis)}}\right]^2\right\}} \quad (11)$$

In order to diminish the number of parameters to be adjusted and bearing in mind what variables were held constant, this expression can be rearranged as follows:

$$(-\hat{r}_{LA}) = \frac{k^*_{(T,\bar{p}_{O2},cat)}}{\left\{1 + K_{LA} \cdot \left[LA_{(dis)}\right] + K_{LB} \cdot \left[LB_{(dis)}\right] + K_r^* \cdot \left[\frac{LB_{(dis)}}{LA_{(dis)}}\right]^2\right\}} \quad (12)$$

It is worth to notice that at t = 0, i.e., for $(-\hat{r}_{LA})^0$, [LB] is zero and [LA] is $[LA]^0$ and Eq. (12) becomes:

$$(-\hat{r}_{LA})^0 = \frac{k^*_{(T,\bar{p}_{O2},cat)}}{\left[1 + K_{LA} \cdot \left[LA_{(dis)}\right]^0\right]} \quad (13)$$

Analyzing the expression obtained for the reaction rate a t = 0, Eq. (13), it can be seen that $(-\hat{r}_{LA})^0$ is constant for a given $[LA_{(dis)}]^0$, in agreement with the experimental evolution observed for each $[LA]^0$ at $X_{LA} < 70$ % (Fig. 5). On the other hand, Eq. (13) predicts that when $[LA]^0$ increases, the resulting initial reaction rate decreases. This conclusion from LHHW is in agreement with the negative order estimated applying the pseudo-homogeneous model. Then, the proposed LHHW model is consistent with the experimental results presented in Fig. 5.

In this case the fittings were performed by minimization of the sum of total square residuals, i.e., (SSR) on Eq. (14), where n stands for all the experimental data, $[LA]_{exp}$ and $[LA]_{calc}$ stand for the experimental and predicted LA concentrations, respectively.

$$(SSR) = \sum_{i=1}^{i=n}\left([LA]_{exp} - [LA]_{calc}\right)^2 \quad (14)$$

We used the general reduced gradient (GRG) algorithm for non-linear optimization problems. The estimates for the kinetic parameters and the corresponding statistical are presented in Table 2.

Except for K_r^*, which will be discussed later, all the estimates for the kinetic parameters are positive and significantly different from zero with a 95 % of confidence (Table 2). In addition, the fitting obtained with this model is acceptably good, i.e., the LHHW predict rather well the experimental data, as it is shown in Fig. 7.

According to the LHHW mechanism proposed in this work, the controlling step of the reaction is the dissociative oxygen adsorption on one active site. The concentration of these active sites depends on the surface concentration of strongly adsorbed LA, which in turn depends on the LA concentration in the liquid phase. In other words, as the LA concentration in the liquid phase is raised, the surface concentration of LA strongly adsorbed increases and the number of surface Au sites available for oxygen chemisorption diminishes [Eq. (6)] and so the initial oxidation rate, which is in agreement with the negative order respect to LA estimated by the pseudo-homogenous modeling.

Finally, it is important to note that the estimate for K_r^* is around 10^{-10} and non-significantly different from zero within a confidence level of 95 %. Then, from Eq. (11) and (12), it was concluded that $K_S \gg 1$. As a consequence, the model is also predicting that the surface reaction, step (iv) from LHHW mechanism, is irreversible. This is in agreement with the experimental results that showed 100 % LA conversion. Therefore, the LHHW model shown in Eq. (12) becomes:

$$(-\hat{r}_{LA}) = \frac{k^*_{(T,\bar{p}_{O2},cat)}}{\left\{1 + K_{LA} \cdot \left[LA_{(dis)}\right] + K_{LB} \cdot \left[LB_{(dis)}\right]\right\}} \quad (15)$$

4 Conclusions

The oxidation rate of lactose in liquid-phase depends strongly on the metal Pt and Au dispersion. In turn, the metal dispersion depends on the oxide used as a support. Thus, the metal dispersion obtained on Pt/Al_2O_3 catalyst is higher than that on Pt/SiO_2 catalyst. Metal nature also has a very strong influence on lactose oxidation rate. It was found that metal Au nanoparticles are much more active than metal Pt particles of similar medium size. As a consequence, the activity pattern found for liquid-phase oxidation of lactose was the following: $Au/Al_2O_3 > Pt/$

Table 2 Kinetic parameters and statistical obtained with LHHW model for the liquid-phase oxidation of lactose on Au(2 %)/Al_2O_3 catalyst considering the dissociative O_2 chemisorption as rate controlling step

Parameter	Estimate	Standard error	Confidence interval[a]	Lower limit	Upper limit
k^*	0.65	0.357	0.20	0.45	0.85
K_{LA}	0.0119	0.00902	0.0050	0.0069	0.0169
K_{LB}	0.0219	0.0231	0.013	0.0091	0.0347
K_r^*	2.5×10^{-10}	3.0×10^{-6}	1.5×10^{-6}	-1.5×10^{-6}	1.5×10^{-6}

[a] Confidence interval at 95 % confidence level

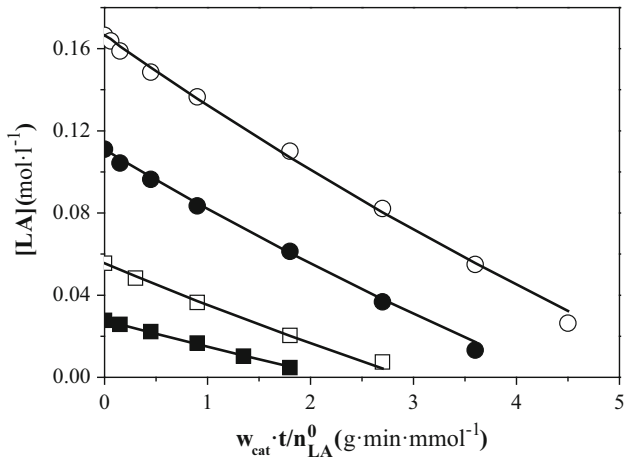

Fig. 7 Lactose concentration, [LA], as a function of parameter $w_{cat} \cdot t/n^0_{LA}$ for different $[LA]^0$, with Au/Al_2O_3 catalyst. T = 65 °C, pH 9.0, $w/n^0_{LA} = 30$ g mol^{-1}. *black square* 0.03 mol L^{-1}; *white square* 0.06 mol L^{-1}; *black circle* 0.11 mol L^{-1}; *white circle* 0.17 mol L^{-1}, *symbols* experimental data; *solid line*: calculated from LHHW model

$Al_2O_3 > Pt/SiO_2$. In addition, Au/Al_2O_3 catalyst is highly selective to lactobionic acid and stable under the reaction conditions used in this work. A kinetic modeling, using a pseudo-homogeneous and a LHHW models, was performed using the experimental data obtained with Au/Al_2O_3 catalyst. In both cases, the kinetic parameters were significantly different from zero with a 95 % confidence. A negative order respect to lactose was estimated by fitting the initial experimental data with the pseudo-homogenous model. This result indicates that lactose is strongly adsorbed on the surface of metal Au nanoparticles. However, for a given initial concentration of lactose, the conversion or reactant varies linearly with time as if the apparent order of reaction respect to lactose were zero. A LHHW model, in which the determining step is assumed to be the dissociative chemisorption of O_2, is compatible with the findings in the pseudo-homogenous modeling. This LHHW model indicates that as the initial lactose concentration was raised, the number of active Au sites available for dissociative oxygen chemisorption diminished and then initial oxidation rate also decreases. Therefore, it was concluded that the kinetic modeling allows to explain the results obtained in the liquid-phase oxidation of lactose over an Au(2 %)/Al_2O_3 catalyst.

Acknowledgments We thank the Universidad Nacional del Litoral (UNL), Consejo Nacional de Investigaciones Científicas y Técnicas (CONICET) and Agencia Nacional de Promoción Científica y Tecnológica (ANPCyT) from Argentina for the financial support of this work. We also acknowledge to LMA-INA-UNIZAR facilities for the transmission electronic microscopy analysis.

References

1. Druliolle H, Kokoh KB, Beden B (1997) Electrooxidation of lactose on platinum and on modified platinum electrodes in alkaline medium. Electrochim Acta 39:2577–2584
2. Gallezot P (2007) Catalytic routes from renewable to fine chemical. Catal Today 121:76–91
3. Budtz P, Vindelev J, Ashie P, Nordkvist M (2005) Enzymatic process for obtained increased yield of lactobionic acid. Canadian Patent WO/2005/104859 A3
4. Meyer N, Devillers M, Hermans S (2015) Boron nitride supported Pd catalysts for the hydrogenation of lactose. Catal Today 241:200–207
5. Gutiérrez LF, Hamoudi S, Belkacemi K (2012) Lactobionic acid: a high value-added lactose derivative for food and pharmaceutical applications. Int Dairy J 26:103–111
6. Murzina EV, Tokarev AV, Kordas K, Karhu H, Mikkola JP, Murzin DY (2008) D-Lactose oxidation over gold catalysts. Catal Today 131:385–392
7. Gangwal VR, van der Schaf J, Kuster BFM, Schouten JC (2005) Influence of pH on noble metal catalysed alcohol oxidation: reaction kinetics and modelling. J Catal 229:389–403
8. Tokarev AV, Murzina EV, Mikkola JP, Kuusisto J, Kustov ML, Murzin DYJ (2007) Application of in situ catalyst potential measurements for estimation of reaction performance: lactose oxidation over Au and Pd catalysts. Chem Eng J 134:153–161
9. Belkacemi K, Vlad MC, Hamoudi S, Arul J (2007) Value-added processing of lactose: preparation of bioactive lactobionic acid using a novel catalytic method. Int J Chem React Eng 5:A64
10. Moroz BL, Pyrjaev PA, Zaikovskii VI, Bukhtiyarov VI (2009) Nanodispersed Au/Al_2O_3 catalysts for low-temperature CO oxidation: results of research activity at the Boreskov Institute of catalysis. Catal Today 144:292–305
11. Uriz I, Arzamendi G, Diéguez PM, Laguna OH, Centeno MA, Odriozola JA, Gandía LM (2013) Preferential oxidation of CO over Au/CuO_x–CeO_2 catalyst in microstructured reactors studied through CFD simulations. Catal Today 216:283–291

12. Shimada S, Takei T, Akita T, Takeda S, Haruta M (2010) Influence of the preparation methods for Pt/CeO_2 and Au/CeO_2 catalysts in CO oxidation. Stud Surf Sci Catal 175:843–847
13. Centeno MA, Hadjiivanov K, Tz V, Hr K, Odriozola JA (2006) Comparative study of Au/Al_2O_3 and Au/CeO_2-Al_2O_3 catalysts. J Mol Catal A 252:142–149
14. Tz V, Hr K, Centeno MA, Odriozola JA, Hadjiivanov K (2006) State of gold on an Au/Al_2O_3 catalyst subjected to different pre-treatments: an FTIR study. Catal Commun 7:308–313
15. Regenhardt SA, Trasarti AF, Meyer CI, Garetto TF, Marchi AJ (2013) Selective gas-phase conversion of maleic anhydride to propionic acid on Pt-based catalysts. Catal Commun 35:59–63
16. Srinivasan R, Davis BH (1992) X-ray diffraction and electron microscopy studies of platinum-tin-silica catalysts. Appl Catal A 87:45–67
17. Bertero NM, Apesteguía CR, Marchi AJ (2008) Catalytic and kinetic study of the liquid-phase hydrogenation of acetophenone over Cu/SiO_2 catalyst. Appl Catal A 349:100–109
18. Bokwon Y, Hannu H, Uzi L (2003) Interaction of O_2 with gold clusters: molecular and dissociative adsorption. J Phys Chem A 107:4066–4071
19. Franceschetti A, Pennycook SJ, Pantelides ST (2003) Oxygen chemisorption on Au nanoparticles. Chem Phys Lett 374: 471–475